Binding Mechanism and Magnetic Properties of a Multifunctional Spin Label for Targeted EPR Imaging of Amyloid Proteins: Insight from Atomistic Simulations and First-Principles Calculations

Xin Li,[*,†] Zilvinas Rinkevicius,[†,‡] Jacob Kongsted,[§] N. Arul Murugan,[†] and Hans Ågren[†]

[†]Department of Theoretical Chemistry and Biology, School of Biotechnology, KTH Royal Institute of Technology, SE-10691 Stockholm, Sweden

[‡]Swedish e-Science Research Center (SeRC), KTH Royal Institute of Technology, SE-10044 Stockholm, Sweden

[§]Department of Physics, Chemistry and Pharmacy, University of Southern Denmark, Campusvej 55, DK-5230 Odense M, Denmark

ABSTRACT: Electron paramagnetic resonance (EPR) imaging techniques provide a promising approach to detect amyloid structures which are of paramount importance in early-stage diagnosis of conformational diseases. Here, we report a combined molecular dynamics and density functional theory/molecular mechanics computational scheme for evaluation of the binding mechanism between a multifunctional spin label and the target amyloid protein. In addition, we consider evaluation of EPR spin Hamiltonian parameters with the aim of providing a better microscopic understanding and interpretation of EPR spectroscopy. The results from molecular dynamics simulations suggest that the oligothiophene conjugate part of the spin label interacts with hydrophobic residues of the amyloid protein through hydrophobic attraction and that both the N−O bond length and the N−O out-of-plane tilt angle in the nitroxide group are slightly diminished after complexation with the protein. The translational and rotational motions of the protein-bound spin label are considerably slowed compared to those of the free spin label in aqueous solution, but interestingly, hydrogen bonds formed between the nitroxide oxygen group and the surrounding water molecules are hardly affected by the presence of the amyloid protein. First-principles calculations suggest that EPR spin Hamiltonian parameters including the nitroxide nitrogen hyperfine coupling tensor $\mathbf{A}^N$ and electronic $\mathbf{g}$ tensor suffer noticeable changes upon complexation with the protein. The magnitude of the $\mathbf{A}^N$ tensor is found to be closely related to the nitroxide N−O out-of-plane tilt angle, while the $\mathbf{g}$ tensor is affected by both the nitroxide N−O bond length as well as the interaction between the spin label and the amyloid protein. With this work we show that state-of-the-art simulation techniques represent a promising way of providing a detailed understanding of the microscopic mechanisms responsible for the formation and stability of a spin label complexed with amyloid structures as well as the magnetic properties of the free and protein-bound spin label.

1. INTRODUCTION

Misfolding and aggregation of proteins, which could take place upon exposure to environmental changes including pH, temperature, glycation, and oxidation, are related to a wide range of diseases which are often highly debilitating.[1,2] Such diseases are recognized as conformational diseases where protein disorders act as the primary causes.[3] The lesion formation process usually starts from the unfolding of native proteins, and by that denatured proteins lose their physiological functions and become thermodynamically unstable, from which aggregations are formed in the search of more stable conformations. Symptoms of neurodegenerative diseases with such origin irreversibly worsen over time by causing progressive deterioration in the structure or function of the affected neurons. It has been observed that the misfolded protein usually forms fibrous aggregates, known as amyloid fibrils, which mainly consist of β-sheets perpendicularly stacked to the filament axis according to the cross-β model.[4] For instance, in Alzheimer's disease the amyloid-β and tau proteins are implicated in formation of senile plaques.[2] Common characterization is pointing out that the disease is marked by the accumulation of amyloid plaques, which consist mainly of extracellular amyloid-β deposits, and formation of neuro-fibrillary tangles, which originate from intracellular deposition

of tau protein.[5] Another example of protein misfolding into amyloid-β structure is insulin, a small peptide hormone that regulates metabolism of carbohydrate and fat. Native insulin consists of two α-helical chains and exists mainly as a biological storage hexamer under neutral pH and the presence of zinc ions; however, formation of inactive amyloid-like fibrils can occur under a variety of conditions which in turn causes diabetes-related problems.[6]

Toward more effective diagnosis and treatment of conformational diseases arising from misfolding of proteins, early detection of formation of fibrillar amyloid deposits is of paramount importance.[7] Nowadays, state-of-the-art diagnostic techniques provide a considerable range of biomarkers with varying levels of accuracy, cost, and availability. Small organic molecules have been utilized as fluorescent probes to monitor the pathological progress of protein aggregation; for example, Lindgren et al.[8] have shown that 4-(dicyanovinyl)julolidine (DCVJ) responds to early formation of oligomeric aggregates of transthyretin and that thioflavin T (ThT) serves as a high-contrast probe toward amyloid fibrils. However, these small molecules are only able to identify a subset of misfolded protein

aggregates, and their relatively rigid structures provide limited flexibility in conformational changes. Nilsson and co-workers[9,10] introduced luminescent conjugated polythiophenes and oligothiophenes as in vitro conformation-sensitive probes in which the flexible thiophene backbone gives rise to the novel property that the spectral signal is related to the conformational change of the molecule.

As an alternative and promising spectroscopic technology, electronic paramagnetic resonance (EPR) imaging provides a very efficient and noninvasive way to monitor both the distribution and the chemical environment of free radicals or spin labels. Since the background concentration of paramagnetic species in tissue is in general very low, the EPR imaging technique is able to provide pictures with high contrast. An early attempt of EPR experiment in a living animal was conducted using X-band measurements,[11] and the L-band technology (in lower frequency than the X-band as required by in vivo measurements) was developed for in vivo imaging later on.[12] More recently, the EPR imaging technique has been employed in an in vivo study of the distribution and metabolism of nitroxide radicals in human skin.[13] Design of novel and highly specific spin labels targeting tissue abnormalities will greatly enhance the applicability of EPR imaging in the detection and monitoring of misfolded protein aggregates in affected tissues. To combine the advantages of both fluorescent probes and electronic paramagnetic spin labels, it is beneficial to integrate the fluorophore (e.g., oligothiophene) and the paramagnetic center (e.g., nitroxide radical) into one molecule, according to the "chromophore–linker–paramagnetic center" concept. It has been demonstrated that oligothiophenes are excellent fluorescent probes for detection of misfolded protein aggregates and that nitroxide radicals are able to provide high contrast in EPR imaging. The combination of these two molecular functional units through a covalent linker is expected to provide a new way toward more efficient and accurate imaging and monitoring of conformational diseases.

For a specific target system, for example, the nitroxide spin label for amyloid structure, the measured EPR spectrum depends on a variety of parameters including temperature, solvent polarity, pH value, viscosity, etc. Therefore, proper interpretation of the EPR spectrum requires detailed knowledge of the interaction among the spin label, the amyloid structure, and the surrounding environment. Such requirements call for state-of-the-art multiscale modeling techniques which provide atomistic information and understanding of the microscopic mechanisms occurring in the nitroxide–amyloid–solvent complex from first principles. The widely used density functional theory/polarizable continuum model (DFT/PCM) approach[14,15] has been found less promising in more complex environments, like mixtures of solvents, liquid crystals, protein surfaces, or cellular membranes, as typically these require explicit inclusion of a large portion of the inhomogeneous environment around the radical, something that dramatically increases the computational cost. More advanced quantum mechanical/molecular mechanical (QM/MM) methods are therefore required in which the interaction between the QM and the MM regions in addition to the electrostatic terms also include polarization/induction as well as other important terms, like charge transfer and exchange-repulsion interactions. Our previous experience[16–18] shows that the hybrid DFT/MM approach allows for an advanced treatment of the coupling between the QM and the MM regions of a system under study

and is capable of consistently accounting for electrostatic Coulomb and polarization/induction interactions between the QM and the MM parts for linear and nonlinear response properties, where the contributions due to the MM region are included in both the Kohn–Sham and the response equations. Such a computational strategy could be employed to study the structures, surface properties, and dynamics of proteins, membranes, and other biological complexes in their native environment in order to design water-soluble spin labels with selective binding affinity to amyloid structures suitable for EPR imaging.

Herein, we focus our efforts on the fluorescent spin label consisting of an oligothiophene chain and a 2,2,6,6-tetramethylpiperidin-1-oxyl (TEMPO) radical covalently bonded via a peptide bond, as shown in Figure 1. Through a
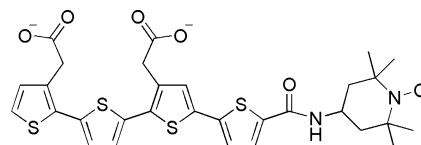
Figure 1. Chemical structure of the spin label under investigation.

combined molecular dynamics (MD) and DFT/MM approach, we studied EPR spin Hamiltonian parameters of the spin label in aqueous solution and in complexation with the insulin amyloid-β sheet. With this work we aim to provide a detailed understanding at the atomistic level of the interaction among the spin label, the amyloid structure, and environmental factors such as solvent molecules and to allow for a direct comparison between EPR spin Hamiltonian parameters of the spin label in free and bound states, thus assisting the interpretation of experimental observations and facilitating rational design of novel fluorescent spin labels with high binding affinity to amyloid protein structures.

2. COMPUTATIONAL DETAILS

The computational approach developed in this work consists of two successive steps. First, classical MD simulations are carried out in order to obtain a sufficient sampling of the interacting structures of the system under investigation. Then a number of snapshots are extracted from the MD trajectories and used as inputs for combined DFT/MM calculations of EPR spin Hamiltonian parameters. The results obtained are finally averaged over the simulation in order to introduce an ensemble average of the parameters. Below we provide a detailed description of the computational procedure.

2.1. Classical MD Simulations. The spin label shown in Figure 1 consists of three parts: an oligothiophene chromophore, a peptide bond linker, and a nitroxide paramagnetic center. The geometry of the spin label was optimized at the unrestricted B3LYP/6-31G* level of theory including solvent effects (water) as described by the polarizable continuum model (PCM).[14,15] These calculations were carried out using the Gaussian09 program package.[20] Using the optimized geometry the electrostatic potential (ESP) of the spin label was calculated at the level of unrestricted B3LYP/cc-pVTZ again with PCM, according to the Merz–Singh–Kollman scheme.[21,22] On the basis of the restrained electrostatic potential (RESP), charges are derived and employed in MD simulations.[23,24] According to previous experience,[19] the force field parameters for the nitroxide paramagnetic center

were taken from the recently developed AMBER force field extension for nitroxide molecules by Barone et al.,[25] and the remainder of the molecule (e.g., the oligothiophene chromophore and peptide bond) was modeled by the General Amber Force Field (GAFF).[24]

The classical MD simulation consists of two parts. The aim of the first part of the MD simulation is to investigate the behavior of the spin label in aqueous solution. The spin label molecule was solvated in a cubic box with dimensions of approximately 43.9 Å by 2773 TIP3P water molecules, and two Na^+ counterions were added to the system as counterions to balance the negative charges of the carboxylate anions. After equilibration the system was simulated using an isothermal–isobaric ensemble (p = 1 atm, T = 298 K) for 50 ns with a time step of 1 fs. After the MD simulation was completed, 80 snapshots were extracted from the last 40 ns trajectory with an equal time interval of 500 ps.

In the second part of the MD simulation, we aim to investigate the binding pattern between the spin label molecule and the insulin β-sheet. Here, the three-dimensional β-sheet model of a C-terminated truncated human insulin was constructed through a residue mutation procedure described by Choi et al.[28] The two chains of the insulin β-sheet consist of 21 and 22 residues, respectively, as shown in Figure 2. The
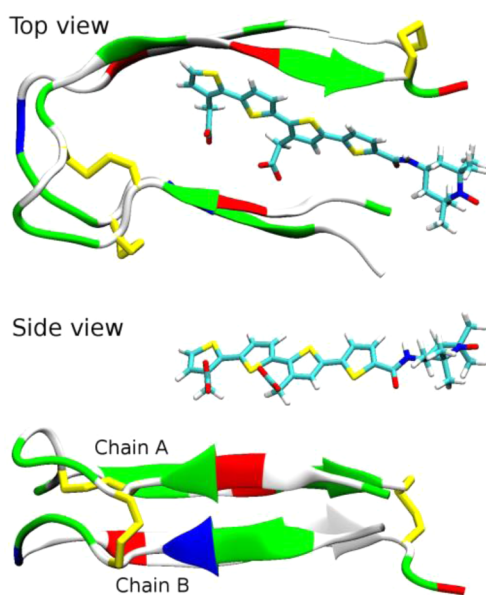
Figure 2. Starting configuration of the spin label and insulin β-sheet. Nonpolar residues, basic residues, acidic residues, and polar residues are shown in white, blue, red, and green, respectively.

AMBER99SB force field[29] was employed to model the insulin β-sheet. The spin label molecule was solvated in a cubic box with dimension of around 65.1 Å together with the insulin β-sheet monomer by 8858 TIP3P water molecules. Five Na^+ ions were added as counterions. The system was simulated using an isothermal–isobaric ensemble (p = 1 atm, T = 298 K) with a time step of 1 fs. Pre-equilibrium simulations started from the configuration shown in Figure 2, during which the spin label molecule was found to bind to the insulin β-sheet through interactions between the oligothiophene and the hydrophobic residues. The simulation was then continued for 50 ns, and 80 snapshots were extracted from the last 40 ns trajectory with an equal time interval of 500 ps.

2.2. DFT/MM Calculations of EPR Spin Hamiltonian Parameters. The EPR spin Hamiltonian parameters of the nitroxide radical, i.e., the electronic **g** tensor and the nitrogen hyperfine coupling tensor (HFC) $\mathbf{A}^N$, were computed by the hybrid DFT/MM approach,[16−18] which has been well developed and extensively benchmarked on the prototypical di-*tert*-butyl-nitroxide compound. According to previous experience,[16−18] the whole spin label molecule was treated as the QM region and the rest of the system consisting of water molecules, the protein, and the ions was designated as the MM region and represented by point charges taken from the force field also used for the MD simulation. For the QM region, the restricted open-shell B3LYP functional was used together with the Huz-III basis set[30,31] for computation of the **g** tensor while the N07D-B3LYP basis set[32] was employed to compute the $\mathbf{A}^N$ tensor. All hybrid DFT/MM calculations were carried out using the development version of the DALTON quantum chemistry program.[33]

3. RESULTS AND DISCUSSION

3.1. Geometrical Structure of the Spin Label. The relationship between geometrical structure and EPR spin Hamiltonian parameters of $R_2NO^\bullet$-type radicals has been under extensive experimental and theoretical studies, and it has been pointed out that the nitrogen hyperfine coupling tensor $\mathbf{A}^N$ depends largely on the out-of-plane tilt angle of the N−O bond. The magnitude of this angle is largely determined through the competition between the sp^3 and the sp^2 hybridization of the nitrogen atom. Furthermore, the electronic **g** tensor is closely related to the N−O bond length.[23,24,34] Figure 3 shows the contour plots of the frontier molecular
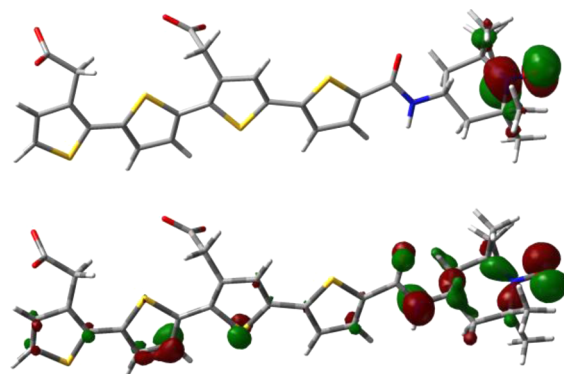

Figure 3. Contour plots of the π-type (top) SOMO and n-type (bottom) MO of the spin label molecule.

orbitals (MOs) of the spin label molecule in an instantaneous snapshot from the MD simulation, calculated at the restricted open-shell B3LYP/cc-pVTZ/PCM level of theory. The π-type singly occupied molecular orbital (SOMO) is mainly localized on the nitroxide radical, while the n-type MO resides in a much lower energy level (the 11th MO below SOMO, or SOMO− 11). As pointed out by several earlier studies,[25−27] the electronic **g** tensor and nitrogen hyperfine coupling tensor $\mathbf{A}^N$ are largely governed by the π-type SOMO and n-type nitroxide oxygen orbital with lone-pair character, and therefore, it is of interest to examine the structural parameters of the $R_2NO^\bullet$ moiety, i.e., the N−O bond length and out-of-plane tilt angle.

As shown in Figure 4, the N−O bond length of the spin label molecule is slightly shortened from 1.29 to 1.28 Å after
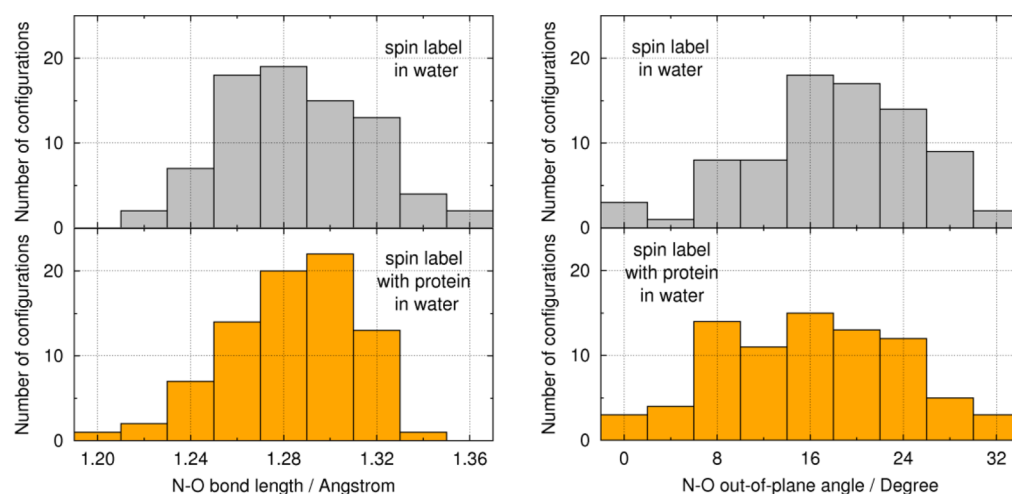
Figure 4. Nitroxide N—O bond length and out-of-plane angle distribution of the spin label molecule obtained from MD simulations.

complexation with the insulin β-sheet monomer. In addition, the distribution of the N—O out-of-plane tilt angle is broadened due to the presence of the protein, and the average tilt angle is also slightly decreased from 18.0° to 16.1°. Overall, the interaction between the spin label molecule and the insulin β-sheet introduces a small but noticeable influence on the geometrical structure of the R$_2$NO$^\bullet$ moiety. It should be noted that the structural parameters of the spin label obtained from the MD simulations are close to those from the QM-optimized structure (see Table 1).

Table 1. Geometrical Structure of Spin Label^a

	N—O bond length/Å	N—O tilt angle/deg
gas phase (QM)	1.29	16.6
in water	1.29 (0.03)	18.0 (7.4)
bound to protein	1.28 (0.03)	16.1 (8.0)

^{a}Standard deviations are given in parentheses.

3.2. Interaction between the Spin Label and Its Environment. Although the presence of insulin β-sheet leads to a relatively small impact on the geometrical structure of the R$_2$NO$^\bullet$ moiety, it will strongly affect the dynamical properties such as the self-diffusion constant and rotational correlation time. To shed light on the interaction between the spin label and the insulin β-sheet, we first examine the root-mean-square deviation (RMSD) of both molecules, as shown in Figure 5. The RMSD of the spin label molecule quickly reaches a plateau of around 1.4 Å, while the RMSD of the protein shows a sudden jump after 6—10 ns of simulation and then oscillates around 4.0 Å. A similar behavior can be seen from the interaction potential energy between the spin label and the protein as shown in Figure 6. Here we decompose the interaction potential energy into two components, i.e., the Lennard—Jones and Coulomb contributions. At the beginning the Coulomb interaction dominates the potential energy; however, at around 8 ns the Coulomb potential energy shifts upward, corresponding to the dramatic change in the RMSD at the same time. Meanwhile, the Lennard—Jones interaction potential energy gradually becomes more negative and starts to contribute dominantly to the potential energy. The dominant role of the Lennard—Jones interaction over the Coulomb interaction suggests that the complexation between the spin
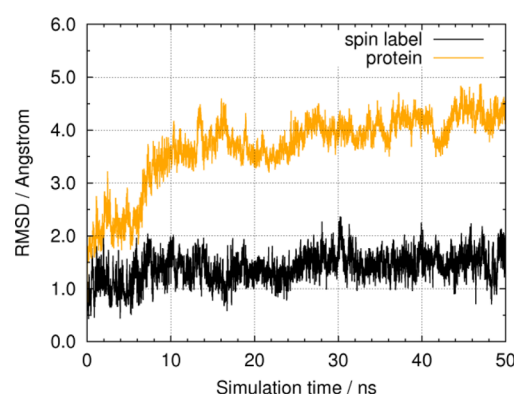
Figure 5. RMSD of the spin label and protein.
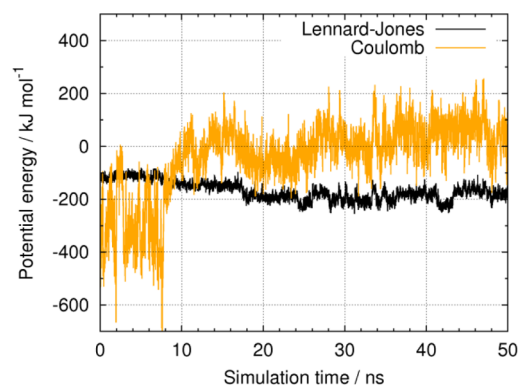
Figure 6. Interaction potential energy between spin label and protein.

label and the insulin β-sheet is driven by hydrophobic interaction arising from nonpolar groups such as alkyl chains and aromatic rings. Figure 7 shows the binding pattern between the spin label and the insulin β-sheet at 8 and 50 ns, respectively; it can be seen that the thiophene rings of the spin label molecule interact with hydrophobic residue side chains and insert into the center of the β-sheet. The interaction potential energy (sum of Lennard—Jones and Coulomb contributions, see Figure 6) increases spontaneously and substantially during 6—10 ns, and such an unfavored increase in potential energy is stabilized by the presence of surrounding water molecules. The nonpolar feature of the interaction
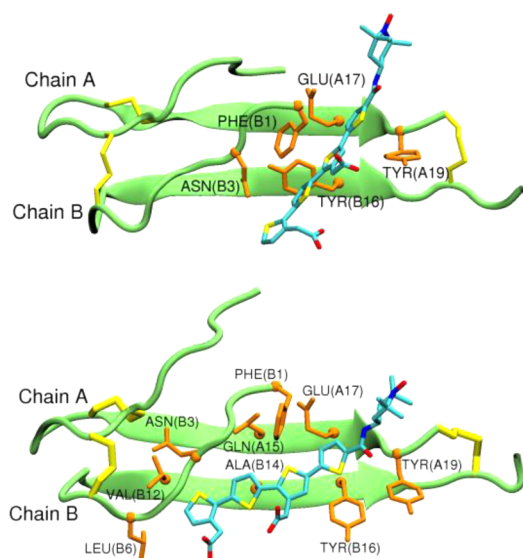
Figure 7. Snapshot at (top) 8 and (bottom) 50 ns.

between the spin label and the protein shows that the complexation process is driven by hydrophobic attractions. The amino acid residues with a large phenyl group (TYR19 on chain A, PHE1 and TYR16 on chain B) are expected to act as recognition sites to initialize the complexation process between insulin β-sheet and spin label molecule. Such a recognition pattern, although demonstrated with a monomer of β-sheet, is also allowed in the insulin fibril model proposed by Choi et al.[28] In this model the cross-sectional area of fibril consists of six parallel-stacked monomer subunits; the recognition sites of insulin β-sheet at the end of fibril are exposed to the environment, and the terminal β-sheet monomer is allowed to deform in order to facilitate complexation with the spin label molecule, as shown in Figure 7.

Dynamical properties related to the spin label molecule before and after complexation with the insulin β-sheet are computed and listed in Table 2. The self-diffusion constant was

Table 2. Dynamical Properties of Spin Label: Self-Diffusion Constant D and Rotational Correlation Time τ[a]

status of spin label	$D/10^{-5}$ cm^2 s^{-1}	τ/ns
in water	0.44 (0.01)	0.135 (0.002)
bound to protein	0.13 (0.02)	1.147 (0.023)

[a]Standard deviations are given in parentheses.

obtained from the derivative of mean square deviation (MSD) according to Einstein's relation, while the rotational correlation time was computed from the rotational correlation function of the normal vector of the plane defined by the nitrogen atom and the two adjacent carbon atoms in the R$_2$NO$^{\bullet}$ moiety. The results suggest that both translational and rotational motions are considerably slowed when the spin label molecule is bound to insulin β-sheet. We also monitored the rotational correlation time of the rigid oligothiophene conjugate and obtained very similar results to those listed in Table 2. The rotational correlation time thus computed is expected to reflect the rotational motion of the whole molecule. In aqueous solution, the correlation time of the spin label is obtained as 0.135 ns, which becomes 1.147 ns after complexation with the protein, with an increase of around 8.5-fold. Clearly the spin label

molecule rotates much slower when it forms a complex with insulin β-sheet; this may result in a notable change in EPR signals.

Beyond the internal dynamics of the R$_2$NO$^{\bullet}$ moiety and host−guest interaction between the spin label and the protein, the environmental influence arising from the surrounding solvent molecules also has an impact on the EPR spin Hamiltonian parameters through direct and indirect mechanisms.[19] Here the numbers of H bonds formed between the nitroxide oxygen atom in the spin label and the surrounding water molecules was analyzed according to structural criteria of $R(ON{-}HW) \leq 2.7$ Å and $R(ON{-}OW) \leq 3.3$ Å,[25] as shown in Figure 8 and Table 3. Here ON denotes the oxygen atom in the
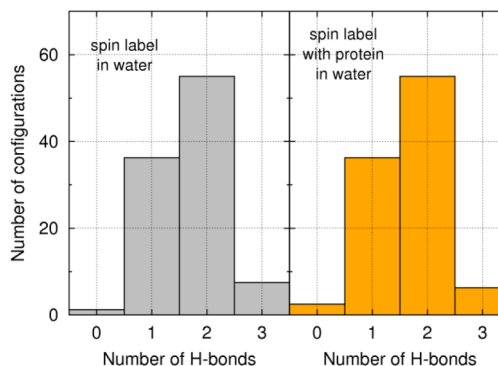

Figure 8. Number of H bonds between the spin label and surrounding water molecules.

Table 3. H Bonds between Spin Label and Surrounding Water Molecules[a]

	status of spin label	
	in water	bound to protein
no. of H bonds	1.69 (0.63)	1.65 (0.64)
$R(ON{-}HW)$/Å	2.04 (0.30)	2.03 (0.38)
$R(ON{-}OW)$/Å	2.87 (0.36)	2.85 (0.48)

[a]Standard deviations are given in parentheses.

spin label, and OW and HW denote oxygen and hydrogen atom in water molecules, respectively. After binding to insulin β-sheet, no obvious change is observed in the number and structure of H bonds formed between the nitroxide oxygen atom in the spin label and the surrounding water molecules; in other words, the number of H bonds is almost unaffected by complexation with the insulin β-sheet, in accordance with the fact that only the oligothiophene part of the spin label molecule has a strong interaction with the protein. Therefore, during the complexation process between the spin label and the protein, the induced changes in the number and structure the H bonds are not expected to give rise to notable variation in EPR spin Hamiltonian parameters of the spin label molecule.

3.3. EPR Spin Hamiltonian Parameters. The first EPR spin Hamiltonian parameter of interest, i.e., the nitroxide nitrogen hyperfine coupling tensor $\mathbf{A}^N$, was computed and averaged over the snapshots taken from the MD trajectories of the spin label in aqueous solution and of the spin label bound to the insulin β-sheet in aqueous solution, respectively. Here the averaging of $\mathbf{A}^N$ was carried out within the Cartesian coordinate system defined by the nitroxide moiety; in Figure 9 we show the three principal axes and values of the $\mathbf{A}^N$ tensor for the case of the spin label bound to the insulin β-sheet in
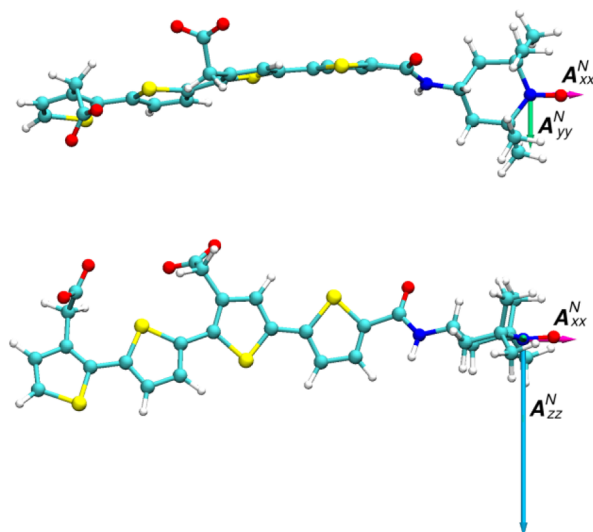
Figure 9. Principal components of averaged nitroxide nitrogen hyperfine coupling tensor $\mathbf{A}^N$ shown in the 25th snapshot taken from the MD trajectory of the spin label bound to the insulin β-sheet in aqueous solution.

Figure 10. Dependence of nitroxide nitrogen isotropic HFCC on N−O out-of-plane angle in snapshots taken from MD trajectory of aqueous spin label.

aqueous solution, where the three principal axes almost coincide with the three Cartesian axes. The magnitude of the principal values is of the following order: $A^N_{xx} < A^N_{yy} \ll A^N_{zz}$, and a similar result was obtained for the average $\mathbf{A}^N$ tensor computed based on the MD trajectory of the spin label in aqueous solution. As we employed the density functional restricted−unrestricted approach,[35] the spin density and spin polarization contributions to the isotropic hyperfine coupling constant (HFCC) were extracted, as listed in Table 4. Clearly,
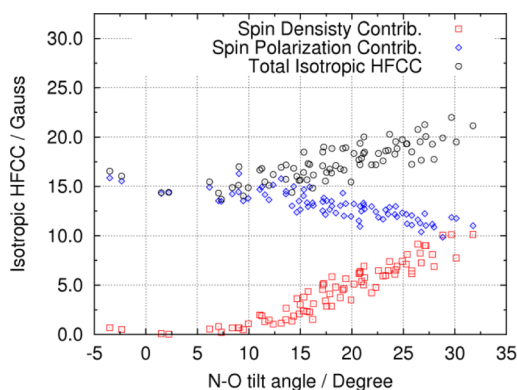
Table 4. Spin Density and Spin Polarization Contributions to Isotropic HFCC of Nitrogen in $R_2NO^{\bullet}$ Nitroxide (in Gauss)[a]

	status of spin label	
contribution	in water	bound to protein
spin density	4.38 (2.79)	3.73 (2.98)
spin polarization	13.03 (1.35)	13.32 (1.40)
total	17.41 (1.88)	17.05 (2.02)

[a]Standard deviations are given in parentheses.

the complexation process between the insulin β-sheet and the spin label gives rise to a decrease in the spin density contribution and an increase in the spin polarization contribution. This is related to the fact that the N−O out-of-plane angle is decreased by 1.9° after complexation with the protein (Table 1). As previously suggested by Rinkevicius et al., the isotropic HFCC of nitrogen in the nitroxide moiety is highly dependent on the N−O out-of-plane motion.[19]

In Figure 10 we plot the dependence of the nitroxide nitrogen isotropic HFCC on the N−O out-of-plane angle computed from snapshots based on the MD trajectory of the spin label in aqueous solution. For a small N−O out-of-plane angle, the spin polarization contribution dominates the isotropic HFCC of nitrogen due to insufficient spin density contribution from the π-type SOMO under a planar configuration. As the N−O out-of-plane angle increases the spin density contribution is enhanced and becomes comparable

to the spin polarization contribution when the out-of-plane angle is around 30° (Figure 10).

We further examined the anisotropy of the nitroxide nitrogen HFC tensor by decomposing the anisotropic $\mathbf{A}^N$ tensor into contributions arising from spin density and spin polarization, respectively, as listed in Table 5. It can be seen that the spin

Table 5. Spin Density and Spin Polarization Contributions to Anisotropy of $\mathbf{A}^N$ in $R_2NO^{\bullet}$ Nitroxide (in Gauss)

status of spin label	contribution	$A^N_{aniso,xx}$	$A^N_{aniso,yy}$	$A^N_{aniso,zz}$
in water	spin density	−8.51	−9.18	17.69
	spin polarization	−0.89	−0.01	0.90
bound to protein	spin density	−8.57	−9.25	17.82
	spin polarization	−0.89	−0.01	0.90

polarization contribution is insensitive to the complexation process with the insulin β-sheet, while the absolute value of the spin density contribution increased a bit, resulting in a slightly enhanced anisotropy of $\mathbf{A}^N$ in the $R_2NO^{\bullet}$ moiety. To summarize, the spin polarization contribution dominates the isotropic nitroxide nitrogen HFCC, while the spin density contribution dominates the anisotropy of $\mathbf{A}^N$ tensor and results in the order $A^N_{xx} < A^N_{yy} \ll A^N_{zz}$.

The second EPR spin Hamiltonian parameter of interest is the electronic $\mathbf{g}$ tensor. The computed $\mathbf{g}$ tensor was averaged over snapshots taken from the MD trajectory according to the coordinate system shown in Figure 9. The principal axes of the $\mathbf{g}$ tensor almost coincide with those of the $\mathbf{A}^N$ tensor; however, the magnitude of the principal component follows the order $g_{xx} \gg g_{yy} \gg g_{zz}$. In the employed DFT/MM approach, the computed $\mathbf{g}$ tensor consists of four contributions, i.e., the free electron g factor, a relativistic mass correction (RMC), a gauge correction (GC) to the electronic Zeeman effect, and a spin−orbit correction coupled with the orbital Zeeman effect (OZ-SO).[36] The last three terms contribute to the shift in the $\mathbf{g}$ tensor, with the major contribution arising from the last term.

In Table 6 we listed the individual contributions to the average shift of the $\mathbf{g}$ tensor computed from the MD trajectories of the aqueous spin label and of the spin label bound to the insulin β-sheet in aqueous solution, respectively. For the $\mathbf{g}$-shift tensor relating to the aqueous spin label, Δg_{xx} and Δg_{zz} are dominated by contributions from OZ-SO and GC, respectively, while Δg_{yy} contains contributions from both terms. The RMC term contributes a negative fraction to the total

Table 6. Contributions to Principal Components and Isotropic Value of g-Shift Tensor (in ppm)^a

component	RMC	GC	OZ-SO	total
		spin label in water		
Δg_{xx}	−273	157	7757	7641 (1042)
Δg_{yy}	−273	1183	3435	4345 (892)
Δg_{zz}	−273	1167	92	986 (1997)
Δg_{iso}	−273	836	3761	4324 (991)
		spin label bound to protein		
Δg_{xx}	−261	502	7149	7390 (1612)
Δg_{yy}	−261	609	2950	3298 (1255)
Δg_{zz}	−261	287	67	93 (2421)
Δg_{iso}	−261	466	3389	3594 (982)

^{a}Standard deviations are given in parentheses.

isotropic g shift. Further inspection reveals a relationship between the **g**-shift tensor and the geometrical structure of the spin label; Figure 11 shows the dependence of the principal
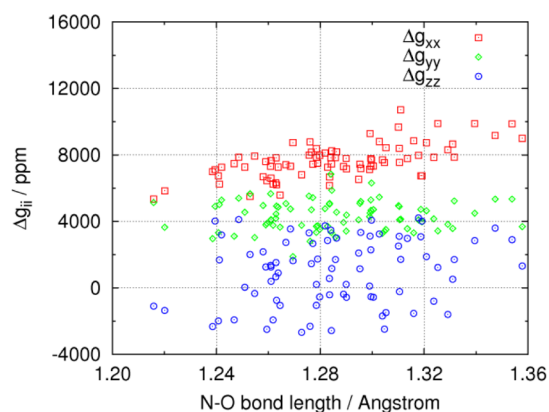
Figure 11. Dependence of the principal components of the shift in the **g** tensor with respect to the N−O bond length in snapshots taken from the MD trajectory of aqueous spin label.

components of the **g**-shift tensor on the nitroxide N−O bond length for aqueous spin label. The magnitude of Δg_{xx} is highly correlated with the N−O bond length, indicating that the OZ-SO contribution is very sensitive to the geometrical change of the nitroxide N−O bond. Kaupp et al. suggested that H bonds can lower the OZ-SO contribution by interacting with the nitroxide oxygen orbital with lone-pair character;[37] however, in our case the H bonds are hardly affected by the complexation process with the protein; therefore, the change in Δg_{xx} and OZ-SO contribution due to the presence of the protein are mainly attributed to the variation of the nitroxide N−O bond length. Differently, Δg_{yy} and Δg_{zz} show no dependence on the nitroxide N−O bond length. It has been reported that Δg_{yy} is less sensitive to the variation of the nitroxide N−O bond length.[37] Finally, Δg_{yy} and Δg_{zz} (especially the latter) contain sizable contributions from the GC term.

In the presence of the protein, the OZ-SO contributions to the **g**-shift components are all diminished due to the slight shortening of the nitroxide N−O bond, while the GC contributions to Δg_{xx}, Δg_{yy}, and Δg_{zz} show different variations compared with those for aqueous spin label, indicating that the GC term is largely affected by the complexation process between the spin label and the insulin β-sheet. The changes in the isotropic g shift induced by the presence of the protein are listed in Table 7. It can be seen that the GC and OZ-SO

Table 7. Changes in Isotropic g Shift (in ppm) Induced by Complexation with Protein

contribution	$\Delta\Delta g_{xx}$	$\Delta\Delta g_{yy}$	$\Delta\Delta g_{zz}$	$\Delta\Delta g_{iso}$
RMC	12	12	12	12
GC	345	−574	−880	−370
OZ-SO	−609	−485	−24	−373
Total	−252	−1047	−892	−730

contribute almost equally to $\Delta\Delta g_{iso}$ and that $\Delta\Delta g_{yy}$ and $\Delta\Delta g_{zz}$ are of major importance among the three principal components. The former consists of comparable contributions from the GC and OZ-SO terms, while the latter consists mainly of contribution from GC. In other words, the complexation process between the spin label and the insulin β-sheet not only diminishes Δg_{zz} by affecting the GC contribution to the **g** tensor but also diminishes Δg_{yy} through a combined effect arising from both the GC and the OZ-SO contributions. Δg_{xx} is much less affected by the presence of the protein. This is due to a partial cancellation between the increase of the GC contribution and the decrease in the OZ-SO contribution.

Experimental EPR measurements of aqueous TEMPO give an HFCC of 17.29 G for the nitrogen atom and an isotropic g shift of 4431 ppm,[38] while the corresponding results from our calculations are 17.41 G and 4324 ppm, respectively. The standard deviation of the computed HFCC for the nitrogen atom is around 2 G, comparable to that obtained from dynamical averaging of atom-centered density matrix propagation trajectory,[39] and it is noteworthy that inclusion of explicit solvent molecules in our DFT/MM approach leads to better agreement between computed results and experimental data. The rationality and reliability of our computational approach has been demonstrated in our previous study on the TEMPO derivative encapsulated by cucurbit[8]uril;[19] in this work the resemblance between experimental data and computed results indicate that very little electronic coupling exists between the oligothiophene fluorophore and the TEMPO spin label. Upon complexation with the insulin β-sheet, the magnitude of HFCC of the nitrogen atom decreased due to the diminished N−O out-of-plane angle, and the isotropic g shift also decreased partially due to the shortening of the nitroxide N−O bond. Furthermore, an 8.5-fold increase was found in the rotational correlation time of the nitroxide moiety, which is expected to result in a notable change in the line shape of EPR spectrum.[40]

4. CONCLUSIONS

The binding mechanism and EPR spin Hamiltonian parameters of a multifunctional spin label designed for targeted EPR imaging of amyloid proteins was studied by means of a combined MD and DFT/MM approach. Through MD simulations it is shown that the interaction potential energy between the spin probe and the amyloid protein consists mainly of the nonpolar Lennard−Jones contribution, indicating the important role of hydrophobic attraction between the oligothiophene conjugate of the spin label and hydrophobic residues of the protein. The presence of the protein results in a slightly shortened nitroxide N−O bond length as well as a slightly narrowed N−O out-of-plane tilt angle, but its impact on hydrogen bonds between the nitroxide oxygen and the surrounding water molecules is almost negligible. Another important effect is that the complexation process with the protein largely diminishes both the translational and the

rotational motions of the spin label molecule, which may give rise to a significant change in the signals of EPR spectroscopy.

With solvent–solute interactions well described by the hybrid DFT/MM approach, EPR spin Hamiltonian parameters are computed with accuracy and reliability. It is found that the nitroxide nitrogen hyperfine coupling tensor $\mathbf{A}^N$ is highly dependent on the N–O out-of-plane tilt angle; at small tilt angles the spin polarization contribution dominates the isotropic hyperfine coupling constant, while the spin density contribution becomes comparable to the spin polarization contribution when the tilt angle increases to around 30°. The anisotropy character of $\mathbf{A}^N$ ($A^N_{xx} < A^N_{yy} \ll A^N_{zz}$) arises mainly from the spin density contribution of the π-type SOMO on the N–O bond. Differently, the electronic $\mathbf{g}$ tensor relies partially on the nitroxide N–O bond length due to the dominant contribution from the OZ-SO term, and its three principal components follow the order $g_{xx} \gg g_{yy} \gg g_{zz}$. Upon complexation between the spin label and the amyloid protein, the GC term is largely affected and contributes similar changes to the isotropic g shift compared with that from the OZ-SO term, which is partially dependent on the N–O bond length.

It is concluded from our multiscale modeling simulations that the hydrophobic part of the spin label shows binding affinity to hydrophobic residues of the amyloid protein and that the complexation process between the spin label and the protein results in an increased rotational correlation time, a decreased isotropic hyperfine coupling constant of the nitroxide nitrogen atom, and a decreased isotropic g shift. Considering the fact that thermodynamic statistics have been taken into account in these simulations, the results obtained connect directly with experiment and provide a microscopic insight and detailed understanding of experimental EPR spectroscopy, which are of great importance for the design of multifunctional spin labels suitable for targeted EPR imaging of amyloid structures and early-stage diagnosis of conformational diseases.

■ AUTHOR INFORMATION

Corresponding Author
*E-mail: lixin@theochem.kth.se.

Notes
The authors declare no competing financial interest.

■ ACKNOWLEDGMENTS

■ ABBREVIATIONS

EPR, electron paramagnetic resonance; DFT, density functional theory; MM, molecular mechanics; MD, molecular dynamics; TEMPO, 2,2,6,6-tetramethylpiperidin-1-oxyl; SOMO, singly occupied molecular orbital; HFCC, hyperfine coupling constant

■ REFERENCES

(1) Chiti, F.; Dobson, C. M. *Annu. Rev. Biochem.* **2006**, *75*, 333−366.
(2) Herczenik, E.; Gebbink, M. F. B. G. *FASEB J.* **2008**, *22*, 2115−2133.
(3) Carrell, R. W.; Lomas, D. A. *Lancet* **1997**, *350*, 134−138.
(4) Schnabel, J. *Nature* **2011**, *475*, S12−S14.
(5) Weiner, H. L.; Frenkel, D. *Nat. Rev. Immunol.* **2006**, *6*, 404−416.
(6) Nielsen, L.; Khurana, R.; Coats, A.; Frokjaer, S.; Brange, J.; Vyas, S.; Uversky, V. N.; Fink, A. L. *Biochemistry* **2001**, *40*, 6036−6046.
(7) DeKosky, S. T.; Marek, K. *Science* **2003**, *302*, 830−834.
(8) Lindgren, M.; Sörgjerd, K.; Hammarström, P. *Biophys. J.* **2005**, *88*, 4200−4212.
(9) Nilsson, K. P. R.; Åslund, A.; Berg, I.; Nyström, S.; Konradsson, P.; Herland, A.; Inganäs, O.; Stabo-Eeg, F.; Lindgren, M.; Westermark, G. T.; Lannfelt, L.; Nilsson, L. N. G.; Hammarström, P. *ACS Chem. Biol.* **2007**, *2*, 553−560.
(10) Åslund, A.; Sigurdson, C. J.; Klingstedt, T.; Grathwohl, S.; Bolmont, T.; Dickstein, D. L.; Glimsdal, E.; Prokop, S.; Lindgren, M.; Konradsson, P.; Holtzman, D. M.; Hof, P. R.; Heppner, F. L.; Gandy, S.; Jucker, M.; Aguzzi, A.; Hammarström, P.; Nilsson, K. P. R. *ACS Chem. Biol.* **2009**, *4*, 673−684.
(11) Feldman, A.; Wildman, E.; Bartolini, G.; Piette, L. H. *Phys. Med. Biol.* **1975**, *20*, 602−612.
(12) Berliner, J. L.; Fujii, H. *Science* **1985**, *227*, 517−519.
(13) He, G.; Samouilov, A.; Kuppusamy, P.; Zweier, J. L. *J. Magn. Reson.* **2001**, *148*, 155−164.
(14) Miertuš, S.; Scrocco, E.; Tomasi, J. *Chem. Phys.* **1981**, *55*, 117−129.
(15) Tomasi, J.; Mennucci, B.; Cammi, R. *Chem. Rev.* **2005**, *105*, 2999−3094.
(16) Olsen, J. M.; Aidas, K.; Kongsted, J. *J. Chem. Theory Comput.* **2010**, *6*, 3721−3734.
(17) Rinkevicius, Z.; Murugan, N. A.; Kongsted, J.; Aidas, K.; Steindal, A. H.; Ågren, H. *J. Phys. Chem. B* **2011**, *115*, 4350−4358.
(18) Rinkevicius, Z.; Murugan, N. A.; Kongsted, J.; Frecuş, B.; Steindal, A. H.; Ågren, H. *J. Chem. Theory Comput.* **2011**, *7*, 3261−3271.
(19) Rinkevicius, Z.; Frecuş, B.; Murugan, N. A.; Vahtras, O.; Kongsted, J.; Ågren, H. *J. Chem. Theory Comput.* **2012**, *8*, 257−263.
(20) Frisch, M. J.; Trucks, G. W.; Schlegel, H. B.; Scuseria, G. E.; Robb, M. A.; Cheeseman, J. R.; Scalmani, G.; Barone, V.; Mennucci, B.; Petersson, G. A.; Nakatsuji, H.; Caricato, M.; Li, X.; Hratchian, H. P.; Izmaylov, A. F.; Bloino, J.; Zheng, G.; Sonnenberg, J. L.; Hada, M.; Ehara, M.; Toyota, K.; Fukuda, R.; Hasegawa, J.; Ishida, M.; Nakajima, T.; Honda, Y.; Kitao, O.; Nakai, H.; Vreven, T.; Montgomery, Jr., J. A.; Peralta, J. E.; Ogliaro, F.; Bearpark, M.; Heyd, J. J.; Brothers, E.; Kudin, K. N.; Staroverov, V. N.; Kobayashi, R.; Normand, J.; Raghavachari, K.; Rendell, A.; Burant, J. C.; Iyengar, S. S.; Tomasi, J.; Cossi, M.; Rega, N.; Millam, J. M.; Klene, M.; Knox, J. E.; Cross, J. B.; Bakken, V.; Adamo, C.; Jaramillo, J.; Gomperts, R.; Stratmann, R. E.; Yazyev, O.; Austin, A. J.; Cammi, R.; Pomelli, C.; Ochterski, J. W.; Martin, R. L.; Morokuma, K.; Zakrzewski, V. G.; Voth, G. A.; Salvador, P.; Dannenberg, J. J.; Dapprich, S.; Daniels, A. D.; Farkas, Ö.; Foresman, J. B.; Ortiz, J. V.; Cioslowski, J.; Fox, D. J. *Gaussian 09*, Revision A.2; Gaussian, Inc.: Wallingford, CT, 2009.
(21) Singh, U. C.; Kollman, P. A. *J. Comput. Chem.* **1984**, *5*, 129−145.
(22) Besler, B. H.; Merz, K. M., Jr.; Kollman, P. A. *J. Comput. Chem.* **1990**, *11*, 431−439.
(23) Bayly, C. I.; Cieplak, P.; Cornell, W.; Kollman, P. A. *J. Phys. Chem.* **1993**, *97*, 10269−10280.
(24) Wang, J.; Wolf, R. M.; Caldwell, J. W.; Kollman, P. A.; Case, D. A. *J. Comput. Chem.* **2004**, *25*, 1157−1174.
(25) Stendardo, E.; Pedone, A.; Cimino, P.; Menziani, M. C.; Crescenzi, O.; Barone, V. *Phys. Chem. Chem. Phys.* **2010**, *12*, 11697−11709.
(26) Pavone, M.; Biczysko, M.; Rega, N.; Barone, V. *J. Phys. Chem. B* **2010**, *114*, 11509−11514.
(27) Pavone, M.; Cimino, P.; De Angelis, F.; Barone, V. *J. Am. Chem. Soc.* **2006**, *128*, 4338−4347.
(28) Choi, J. H.; May, B. C. H.; Wille, H.; Cohen, F. E. *Biophys. J.* **2009**, *97*, 3187−3195.
(29) Hornak, V.; Abel, R.; Okur, A.; Strockbine, B.; Roitberg, A.; Simmerling, C. *Proteins: Struct., Funct., Bioinf.* **2006**, *65*, 712−725.

(30) Schindler, M.; Kutzelnigg, W. *J. Chem. Phys.* **1982**, *76*, 1919–1933.

(31) Helgaker, T.; Jaszuński, M.; Ruud, K.; Górska, A. *Theor. Chem. Acc.* **1998**, *99*, 175–182.

(32) Barone, V.; Cimino, P.; Stendardo, E. *J. Chem. Theory Comput.* **2008**, *4*, 751–764.

(33) http://www.daltonprogram.org (accessed July 3, 2012)

(34) Improta, R.; Barone, V. *Chem. Rev.* **2004**, *104*, 1231–1254.

(35) Rinkevicius, Z.; Telyatnyk, L.; Vahtras, O.; Ågren, H. *J. Chem. Phys.* **2004**, *121*, 7614–7623.

(36) Rinkevicius, Z.; Telyatnyk, L.; Sałek, P.; Vahtras, O.; Ågren, H. *J. Chem. Phys.* **2003**, *119*, 10489–10496.

(37) Asher, J. R.; Doltsinis, N. L.; Kaupp, M. *J. Am. Chem. Soc.* **2004**, *126*, 9854–9861.

(38) Bardelang, D.; Banaszak, K.; Karoui, H.; Rockenbauer, A.; Waite, M.; Udachin, K.; Ripmeester, J. A.; Ratcliffe, C. I.; Ouari, O.; Tordo, P. *J. Am. Chem. Soc.* **2009**, *131*, 5402–5404.

(39) Caruso, P.; Causà, M.; Cimino, P.; Crescenzi, O.; D'Amore, M.; Improta, R.; Pavone, M.; Rega, N. *Theor. Chem. Acc.* **2012**, *131*, 1211.

(40) Hommel, H. *Adv. Colloid Interface Sci.* **2008**, *141*, 1–23.